Exp Astron
DOI 10.1007/s10686-016-9491-4

ORIGINAL ARTICLE

ChemiX: a Bragg crystal spectrometer for the *Interhelioprobe* interplanetary mission

M. Siarkowski[1] · J. Sylwester[1] · J. Bąkała[1] · Ż. Szaforz[1,2] · M. Kowaliński[1] · Z. Kordylewski[1] · S. Płocieniak[1] · P. Podgórski[1] · B. Sylwester[1] · W. Trzebiński[1] · M. Stęślicki[1] · K. J. H. Phillips[3] · O. V. Dudnik[4] · E. Kurbatov[4] · V. D. Kuznetsov[5] · S. Kuzin[6] · I. V. Zimovets[7]

Received: 22 October 2015 / Accepted: 3 January 2016

Abstract *Interhelioprobe* (IHP), an analogue to the ESA *Solar Orbiter*, is the prospective Russian space solar observatory intended for in-situ and remote sensing investigations of the Sun and the inner heliosphere from a heliocentric orbit with the perihelion of about 60 solar radii. One of several instruments on board will be the Bragg crystal spectrometer ChemiX which will measure X-ray spectra from solar corona structures. Analysis of the spectra will allow the determination of the elemental composition of plasma in hot coronal sources like flares and active regions. ChemiX is under development at the Wrocław Solar Physics Division of the Polish

✉ Ż. Szaforz
zs@cbk.pan.wroc.pl

M. Siarkowski
ms@cbk.pan.wroc.pl

K. J. H. Phillips
kennethjhphillips@yahoo.com

O. V. Dudnik
dudnik@rian.kharkov.ua

V. D. Kuznetsov
kvd@izmiran.ru

S. Kuzin
kuzin@lebedev.ru

I. V. Zimovets
ivanzimovets@gmail.com

[1] Space Research Centre, Polish Academy of Sciences, Kopernika 11, 51-622 Wrocław, Poland

[2] Astronomical Institute, University of Wrocław, Kopernika 11, 51-622 Wrocław, Poland

[3] Earth Sciences Department, Natural History Museum, London SW7 5BD, UK

Published online: 22 January 2016

Academy of Sciences Space Research Centre in collaboration with an international team (see the co-author list). This paper gives an overview of the ChemiX scientific goals and design preparatory to phase B of the instrument development.

Keywords Flares, Spectrum · Spectral line, intensity and diagnostics · Spectrum, X-ray

1 Introduction

The *Interhelioprobe* and *Solar Orbiter* (SolO) projects are currently being developed by the Russia and the European Space Agency [27, 28] respectively. Through multiple gravitational maneuvers near Venus, the *Interhelioprobe* spacecraft will gradually approach the Sun to $\sim$ 60 solar radii. At this location it will achieve nearly co-rotation with the solar surface. The orbital plane will be inclined up to 30° to the plane of the ecliptic through the gravitational maneuvers. The main objectives of the IHP and SolO missions are studies of the fine structure and dynamics of solar atmosphere, the solar coronal heating processes and solar wind acceleration mechanisms, the properties of the inner heliosphere plasmas in regions that have not yet been explored by modern spacecraft and to study polar and equatorial regions from high solar latitudes. The two IHP missions are planned to be launched using Soyuz-Fregat launchers in 2025 and 2026 respectively as at mid 2015.

A few years ago, the Wrocław Solar Physics Division of Polish Academy of Sciences Space Research Centre was offered the possibility of joining both Russian missions with a novel Bragg crystal spectrometer devoted to study the composition of coronal plasma by remotely sensing the coronal X-ray spectra.

From such a close vantage point at perihelion, the solar surface will be observed with a spatial resolution $\sim$ 4 times better than was possible before with the solar radiative fluxes up to 13 times greater than from Earth distance. Both IHP spacecraft will carry identical $\sim$ 150 kg science payloads consisting of approximately 20 scientific instruments [23, 24]. A schematic view of the IHP satellite is given in Fig. 1.

The spacecraft, under design at the Lavochkin Research and Production Association in Russia, will be 3-axis stabilized, pointing to the centre of the solar disk to within 1 arcmin. The pointing drift rate will be less than 1 arcsec/s in all three axes. The maximum telemetry downlink rate will be 1 GB/24h. During the initial phase

[4] Institute of Radio Astronomy, NASU, Chervonopraporna St, 4, 61022 Kharkiv, Ukraine

[5] Institute of Terrestrial Magnetism and Radiowave Propagation (IZMIRAN), Troitsk, Moscow, Russia

[6] Lebedev Physical Institute, Russian Academy of Sciences, Leninsky Prospekt 53, Moscow, 119991, Russia

[7] Space Research Institute, Russian Academy of Sciences, Profsoyuznaya ul. 84/32, Moscow, 117997, Russia

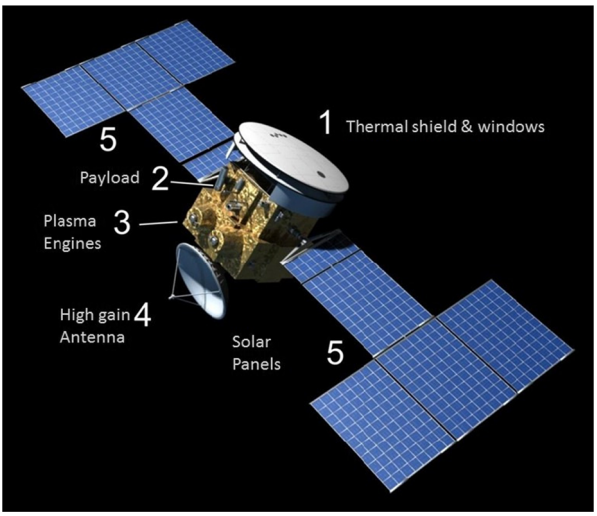

Fig. 1 Schematic view of the *Interhelioprobe* with the main satellite systems annotated. The size of the spacecraft is approximately 3.7 × 4.5 × 3.7 m

of the flight, plasma engines will be used in order to shorten the time to reach final elliptical orbit. Numerous Venus gravity assist maneuvers will allow the inclination of the orbit to be changed by 6 degrees on each maneuver. The projected lifetime of the mission will be at least 5 years.

The general concept of the IHP missions is to perform:

– Multi-wavelength solar observations at small distances from the Sun (down to 60 $R_{\odot}$).
– Out-of-ecliptic observations of the solar atmosphere, in particular polar regions, and observations of the Sun surface not directly seen from Earth.
– In situ measurements at the inner heliosphere plasma in and out of the ecliptic plane.

These measurements are to be performed from two different spacecraft to allow a stereoscopic view of the Sun.

The science goals covered by scientific instruments are:

1. Investigations of magnetic fields in the solar polar regions to help understand the solar dynamo mechanism and solar cycle.
2. Studies of fine details and dynamics of the solar atmospheric structures.
3. Investigations of mechanisms of solar coronal heating and acceleration of the solar wind.
4. Studies of the nature and global dynamics of the most powerful manifestations of the solar activity – solar flares and associated coronal mass ejections and solar energetic particles – and their influence on the heliosphere and space weather.
5. Studies of processes of generation and transport of energetic particles at the Sun and in the heliosphere.

The ChemiX bent crystal spectrometer will contribute to the science tasks numbers 2, 3, 4, and 5 in the above.

2 The ChemiX instrument

Shortly after the successful flight of RESIK [42] aboard the *CORONAS-F* satellite, our group initiated work on the design of a follow-on instrument with improved capabilities, aimed at studies of coronal plasma properties and composition based on interpretation of the observed X-ray spectra. It was realized that, for an instrument placed into Low Earth Orbit (LEO), we would need to use quite large crystals, approximately 20 cm $\times$ 5 cm, in order to collect a significant spectral signal. Position sensitive detectors also should have appropriate large sizes. The mass of such an instrument would be approximately 20 kg, while the cost of the crystals alone would be hundreds of thousands of Euros. Such an instrument could not be supported by Polish resources alone. However, our Russian colleagues offered the possibility of placing a crystal spectrometer with the required specifications on board the *Interhelioprobe* interplanetary mission which would approach the Sun to a distance from which photon fluxes would be an order of magnitude larger than from 1 AU. This would allow much smaller crystals and detectors to be used. Accordingly, the Polish National Science Centre has awarded the necessary resources for a phase B development of the instrument.

ChemiX (**Chem**ical composition **i**n **X**-rays) is a versatile X-ray Bragg spectrometer, designed to use multiple bent, convex crystals forming 10 independent spectral channels, each equipped with a CCD detector for measuring diffracted X-ray spectra of quiet, active and flaring coronal structures. The spectral range will be from 1.5 Å to 9 Å in four slightly overlapping bands, with a spectral resolution of 5 – 7 times better than its predecessor RESIK whose spectral range was 3.4 – 6.1 Å. In addition, the ChemiX signal-to-noise ratio will exceed that of RESIK by a factor 3 – 5, allowing reliable measurements of the continuum over the entire spectral range. In addition, a special X-ray arrangement [41] of the crystal-detector units – a so called dopplerometer configuration, will enable spatial and Doppler motions to be distinguished in three plasma temperature ranges. Radial plasma motions will be determined in the absolute reference system calibrated using the projected motion of the spacecraft (S/C) relative to the Sun, while studies of changing line profiles will lead to estimates of the emitting plasma turbulent velocities. To our knowledge, ChemiX is the only Bragg solar soft X-ray spectrometer planned for operation during Solar Cycle 25/26.

The geometry of X-rays in the two spectrometer units of ChemiX is given in Fig. 2. A similar geometry is used for the dopplerometer sections.

2.1 ChemiX objectives

Solar X-ray spectroscopy had a "golden age" in the 1980s, when several space missions were launched having Bragg crystal spectrometers. These included two on the *Solar Maximum Mission* (SMM; [1]) – a finely collimated scanning *Flat Crystal*

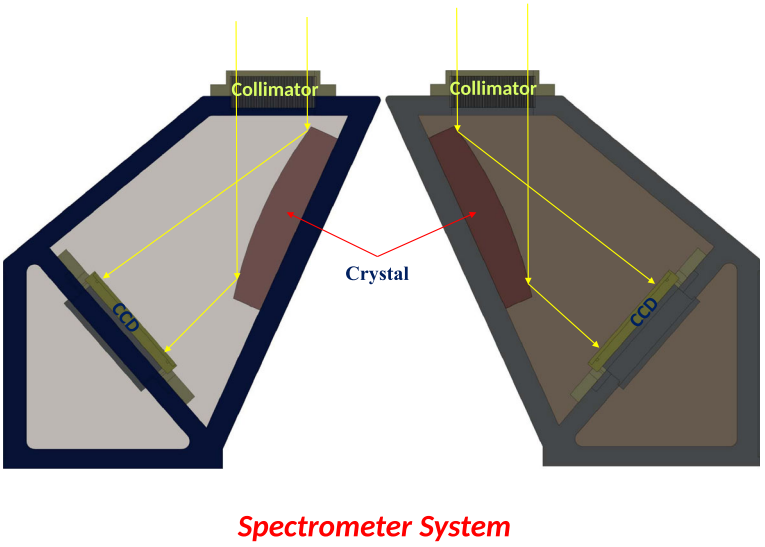

Fig. 2 The crystal-detector geometry with X-ray paths (*yellow*) in the two ChemiX spectrometer units (channels). A similar geometry will be used in the dopplerometer mode, with identical crystals in each pair but with opposite sense of dispersion

Spectrometer (FCS) and the *Bent Crystal Spectrometer* (BCS). The BCS on SMM as well as the similar Bragg Crystal Spectrometer on the follow-up Japanese JAXA mission *Yohkoh* [7] had very high spectral resolution (crystals with large radii of curvature). With position-sensitive gas detectors, instantaneous measurement of spectra over the entire range is possible. Spectral resolution can also be traded with the amount of spectral coverage with on-board software. A disadvantage is that only relative Doppler shifts due to moving plasma such as in flares can be measured since the positions of emission along the detector anode wire are a function of not only wavelength but also source position within the field of view – in the case of the SMM BCS, this was defined by a grid collimator with 6 arcmin FWHM field of view (FOV). The SMM FCS developed problems with the spectral scanning drive early in the mission so a limited number of spectral scans were obtained. For flares, scanning flat crystal spectrometers have the disadvantage that time variations of emission during flares particularly are folded with wavelength-dependent variations so interpretation of spectra is often compromised. The X-ray crystal spectrometers on the Japanese *Hinotori* mission [47] and the US Naval Research Laboratory's *P78-1* spacecraft [8] obtained high-resolution spectra in the region of the Fe XXV and Fe XXVI lines which are emitted at very high flare-associated temperatures. Spectrometers on early Russian spacecraft observed active-region and flare-associated emission from the Mg XI triplet (9.14 – 9.33 Å) [21, 34] and Mg XII Lyα doublet (8.421 Å; [19, 36]). More recently, the RESIK bent crystal spectrometer on the Russian *CORONAS-F* spacecraft covering the range 3.4 – 6.1 Å [42] has taken about 2 million spectra, and many analyses of spectra have been made. Even now, only 10 000 of them have been

reduced to science grade (so-called Level_2: see www.cbk.pan.wroc.pl/experiments/resik/RESIK_Level2/index.html).

So far, after about 50 years of the solar X-ray emission studies, the status of the experimental research in this area is still unsatisfactory. In spite of substantial efforts, it has not been possible to cover systematically the entire range of solar soft X-ray emission. Notwithstanding these shortcomings, important knowledge has been gained based on interpretation of these measurements. Attention has been focused mostly on H, He and Ne-like spectra of solar-abundant elements: Fe, Ca, Ar, S, Si, Mg, Ne, Na, and O. A brief summary of the major results from analysis of the X-ray spectra from these instruments can be given as follows:

a Spectral lines are turbulently broadened during the early phase of flares [16, 18], with no apparent centre-to limb effects.
b Separate spectral line components shifted to shorter wavelengths with respect to the main thermal line are present during the initial phases of flares. Because of a strong centre-to-limb variation, these "blue-shifted" line components can be explained by upflowing plasma "evaporated" during the flare impulsive phase [3, 15, 50].
c In at least one case (an intense X-class flare), entire line Doppler shifts have been noted [31].
d The K_α and K_β line emission arising from fluorescence of photospheric material has a substantial centre-to-limb effect [29].
e Relative emission line intensities indicate a multi-temperature character of the coronal plasma sources, both in flares and non-flaring active regions [38–40].
f Analyses of X-ray lines indicate that flare and active-region plasma element abundances differ from photospheric abundances by amounts that depend on element first ionization potentials [30, 37, 40, 44–46].
g Observed satellite and resonance line ratios indicate the presence of non-Maxwellian distributions (in particular kappa (κ) or n-distributions) of electrons in flare plasmas [14, 22].

The proposed ChemiX spectrometer is very much a part of the heritage of the above X-ray spectrometers, but the spectra that will be obtained should have at least a factor-of-10 improvement in the spectral resolution over that of RESIK and have a larger spectral range (up to 9 Å). The instrument will be able to observe targets like active regions and flares, all to be selected automatically by an on-board computer using images of the soft X-ray corona obtained with a pin-hole imager, an integral part of ChemiX. The use of cooled CCD detectors to record the spectra will result in an order-of-magnitude increase of the continuum-to-background signal, as compared with RESIK. This will improve the precision of absolute abundance determinations by at least a factor of three, which we consider to be the main scientific goal of ChemiX. Indeed, for some elements, the accuracy of abundance determinations should be at least as high as those from optical spectra. This will have much relevance in the context of helioseismology [2, 33], FIP-dependent differentiation [25, 26, 48] and power radiation losses from plasmas [5]. Studies of the intensity ratio of X-ray dielectronic satellite lines to resonance lines during flares may lead to

the diagnosis of electron energy distributions in the 2 – 10 keV energy range and so the detection of non-Maxwellian effects and the lower energy limit of the distribution of non-thermal electrons that give rise to hard X-ray emission during the impulsive phase of flares.

The main scientific goal of ChemiX is however the determination of elemental composition of solar coronal plasma structures that are bright in X-rays. Elemental abundances will be determined from analysis of their high-resolution, collimated spectra. In the analysis of such spectra the most up-to-date versions of spectral software packages like CHIANTI is to be used: http://www.chiantidatabase.org/. In addition, the following quantities characterizing the physical conditions prevailing in individual coronal structures will be derived or determined:

a Thermal (ion temperature) and turbulent line widths, and their time variations in flares and ARs.
b Directed plasma motions of key plasma constituents like Si, S, Ar, Ca, Fe (for the first time the absolute velocity determinations will be possible thanks to the flight-proven X-ray dopplerometer configuration).
c Multi-temperature structure of the thermal plasma will be studied, for the first time based on hundreds (not just tens) of temperature-sensitive lines, including transitions in multiple H- and He-like resonance line sequences extending to spectral components corresponding to $n \sim 10$ transitions.
d Information on the energy distribution of electrons in the 2 – 10 keV range in the event of small departures from Maxwellian distributions, based on dielectronic satellite-to-parent line intensity rates.

The measurements will be made from two vantage points and will be supported by observations made from other spacecraft and from ground-based instruments.

3 Design of the ChemiX spectrometer and dopplerometer

The ChemiX 1.5 – 9 Å spectral range will be covered by four crystal–detector units placed side by side. Mono-crystal wafers bent cylindrically to a desired radius of curvature will be used. The spectral coverage for individual crystals was selected through the development of crystal ray-tracing software connecting the angle of incidence on the crystal with the position of the Bragg-reflected ray on the CCD. Experience from the design of the RESIK instrument was helpful, but the geometry problem here was more complicated while no direct method of "inversion" is analytically possible since solutions to sixth-order equations are required. The details of the ray tracing problem are given in the Appendix A and B. Using the software described there, we selected the set of crystals for the spectrometer: Si, Quartz, KDP and KAP crystals. The amount of X-ray fluorescence produced by irradiance of solar X-rays of the crystal material, which commonly forms a background emission, is minimized for these crystals. The wavelength ranges for these four crystals are 1.500 – 2.713 Å, 2.700 – 4.304 Å, 4.290 – 5.228 Å and 5.200 – 8.800 Å respectively; the slight overlap of each range enables a cross-calibration check. Table 1 gives a summary of the

Table 1 ChemiX spectral channels

Channel No.	Crystal	Diffracting plane	$2d$ [Å]	Wavelength range [Å]	Av. spectral resolution [mÅ per pixel]	Curvature radius [mm]	Crystal length [mm]	Crystal width [mm]	Number of crystals
Spectrometer channels									
1	Si	111[a]	6.271	1.500–2.713	1.41	176.000	46.5	10.0	1
2	Quartz	$10\bar{1}0$	8.514	2.700–4.304	1.82	166.729	44.8	10.0	1
3	KDP	011	10.185	4.290–5.228	0.98	410.425	53.5	10.0	1
4	KAP	001	26.64	5.200–8.800	4.2	364.731	61.7	10.0	1
Dopplerometer channels									
5, 6	LiF	022	2.848	1.835–1.949	0.12	650.0	46.1	10.0	2
7, 8	Si	111[a]	6.271	3.150–3.324	0.11	2500.0	58.2	10.0	2
9, 10	Si	111[a]	6.271	3.900–4.080	0.19	1000.0	47.0	10.0	2

[a]Even orders of reflection do not occur

four channels. The table also includes data for the X-ray dopplerometer described below [see e.g. 43].

The principle of the dopplerometer is shown in Fig. 3. Two cylindrically bent crystals C_1 and C_2 Bragg diffract the flare X-ray emission initially at location A on the Sun. A strong emission line at wavelength λ_0 is sensed on the CCD detectors D_1 and D_2. The bin positions where the line peak is detected (b1 and b2) fulfil the Bragg condition $\lambda = 2d \sin\theta$. The directions of increasing wavelength on both detectors increase in the direction of the thin purple arrows (upwards in the Fig. 3). If the flare emission moves from location A to location B along the plane of dispersion of the crystal, the Bragg condition is fulfilled lower down on crystal C_1 but higher up on C_2. Thus, the apparent bin position corresponding to the line peak moves in opposite directions along both detectors as indicated by the thicker short green arrows. For an X-ray flare stationary at location A but with plasma moving radially towards the observer, the line peak is Doppler-shifted to shorter wavelengths, and the emission is shifted downwards on both detectors. This "dopplerometer" mode is therefore able to distinguish between proper motions and Doppler shifts of flare X-ray emission. On ChemiX, the dopplerometer section will consist of three pairs of crystal – detector units. Crystals in each pair are intended to be identical as far as practically possible (see Table 1), except being oriented in opposite directions. It will allow the observation of highly ionized lines of Fe ($\sim$ 1.85 Å), Ca ($\sim$ 3.2 Å) and Ar ($\sim$ 3.9 Å).

Figure 4 shows examples of simulated spectra from channels 1 and 4. This simulation assumes plasma with temperature $T_e \approx 18.7$ MK and emission measure $EM \approx 5.6\ 10^{49}$ cm^{-3} i.e. conditions corresponding to a typical *GOES* M5 class solar flare. Collimator and CCD efficiencies are assumed to be unity. Spectral atlases consisting of full spectral scans over the entire 1.5 – 9 Å range will be taken while

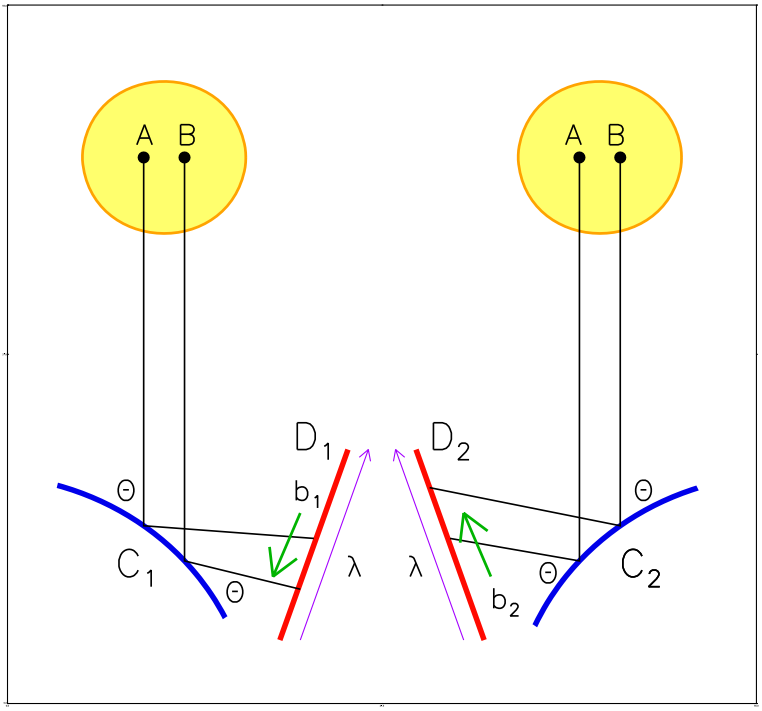

Fig. 3 The principle of the ChemiX dopplerometer. The instrument consists of a pair of curved crystals (C_1, C_2) which view line emission from a solar X-ray-emitting region which moves from **A to B**. The diffracted radiation is sensed by CCD detectors D_1 and D_2, with long *purple arrows* indicating increasing wavelengths along the dispersion direction. Doppler shifts to shorter wavelengths due to radial motions towards the observer give rise to line shifts downwards on both detectors, while spatial shifts from location **A** to location **B** give rise to line shifts downwards on detector D_1 but upwards on detector D_2

the instrument is directed at a particular source with a user-chosen total count level (e.g. a total of 10 000 photon counts over the spectrum in a given spectral channel). Spectral line and continuum fluxes will be obtained with unprecedented precision, especially when the spacecraft is at perihelion, about 0.3 AU from the Sun when the photon fluxes presented in Fig. 4 will be >10 times higher.

4 ChemiX construction

Because of the proximity to the Sun at spacecraft perihelion in its highly elliptical orbit, it has been possible to make the bent crystal spectrometer much more compact and lighter than Earth-orbiting spectrometers with similar sensitivity. The design of the ChemiX must comply with the requirements (described in respective Roskosmos documents) that are more stringent than those necessary to accomplish space missions in Low Earth Orbits. In particular, the instrument must survive the conditions of strong solar thermal illumination, up to 13 times larger than at the 1 AU distance.

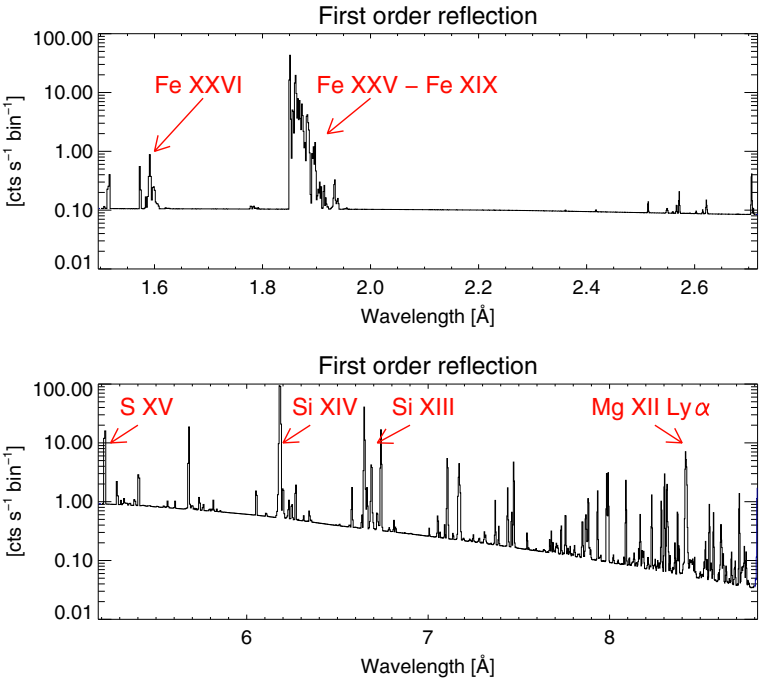

Fig. 4 Simulated spectra as seen on the CCD calculated for a Sun – spacecraft distance of 1 AU using the CHIANTI database. *Top panel* spectrometer channel **1** spectrum with Fe XXV and Fe XXIV dielectronic satellites. *Lower panel* spectrometer channel **4** spectrum that consist mostly of high ionized Si and S and Mg lines

The instrument must also operate for approximately 10 years while the spacecraft travels in its highly eccentric orbit with distances from the Sun varying from ~ 0.3 to ~ 0.7 AU.

The instrument concept is shown in Figs. 5 and 6. Figure 5 shows the location of the ChemiX measurement block (MB) on the *Interhelioprobe* spacecraft, behind the shield of thermal and ultraviolet filters (TUVF). Figure 6 shows details of the measurement block components with the configuration of the spectrometer and dopplerometer crystal – detector units indicated. The total mass of ChemiX is ~ 6 kg, average power consumption 10 W, and the telemetry rate always more than 20 MB/day (the approximate average will be 60 MB/day). The size of the measurement block is $30 \times 30 \times 24$ cm and it is placed ~ 1 m behind systems of two TUVF filters.

Other subsystems of ChemiX include:

– the background particle monitor system (BPM), i.e. detector of energetic particles (electrons, protons, and light nuclei), so that the instrument will have its own monitor installed for safety concerns with the electronics,
– a soft X-ray pin-hole camera with CCD detector, providing instant X-ray context images with one-arcmin spatial resolution providing contextual information on active region and flare locations and flare trigger,

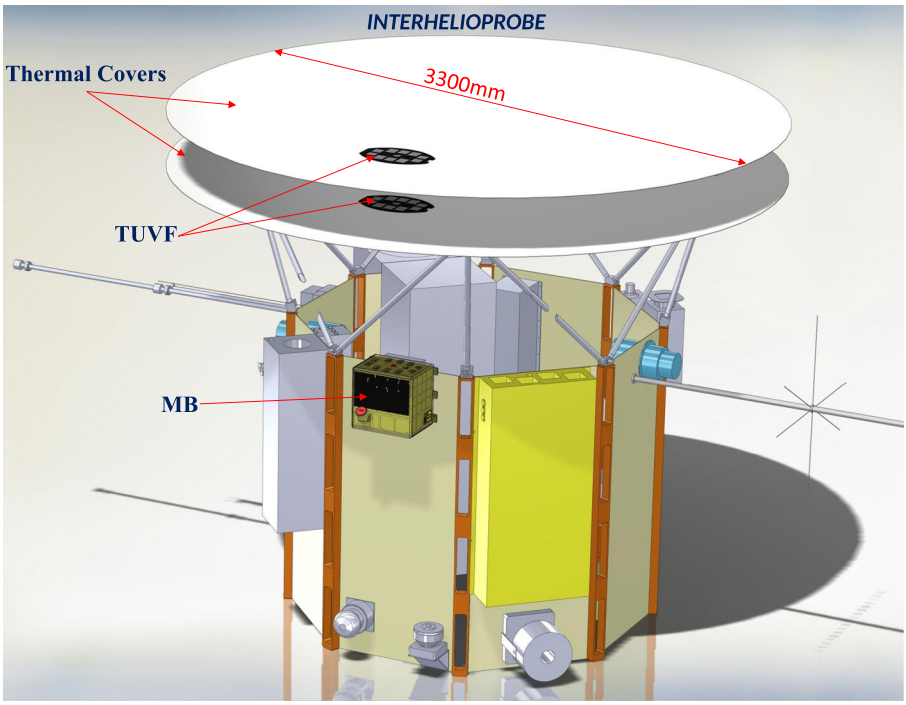

Fig. 5 ChemiX measurement block (MB) with crystal–detector sections location within the IHP spacecraft, behind the set of eleven thermal and ultraviolet filters (TUVF)

- a movable target-pointing platform, on which crystals and detectors are placed, that can lock the spectrometer to a particular flare or other region within seconds of a flare trigger obtained from pin-hole CCD,
- a pair of thermal filters placed within the S/C thermal shield in front of the instrument entrance aperture which will block undesirable solar thermal, ultraviolet and soft X-ray radiation (above 10 Å).

4.1 The Background Particle Monitor (BPM)

The Background Particle Monitor is a semi-autonomous module within ChemiX which will observe the high energy charged particles fluxes of solar origin as well as interplanetary cosmic rays. The particle flux to be measured by the BPM may increase substantially due to passing clouds of solar energetic particles (SEP) accompanying flares or coronal mass ejections (CMEs). Enhanced particle fluxes with changing energy spectra may penetrate the instrument shielding reaching CCDs in the spectrometer module. This will affect the usual ChemiX regular X-ray measurements resulting in enhanced background levels. The BPM measurements of background particle flux intensity will be able to indicate time periods when there is increased particle flux. For exceptionally high levels of particle flux detected by the BPM a dedicated flag will be used to switch off the ChemiX instrument or some

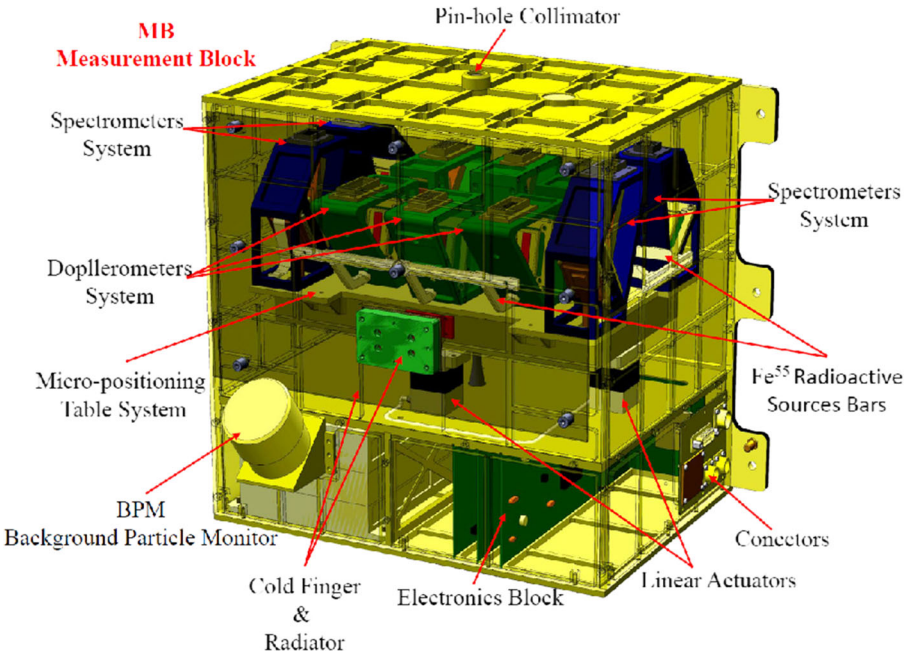

Fig. 6 Details of ChemiX measurement block internal configuration (see text)

of its sensitive subsystems to prevent their damage. As the BPM needs to operate independently of ChemiX state (including power off state), the monitor has a dedicated power supply line. The overall design of BPM and block diagrams of individual sections are shown in Fig. 7.

Thanks to a special design of the detector head, the BPM will also provide scientific data on the type and energies of the detected particles. The BPM's detector head consists of three-layer sensor stack placed behind conical collimator limiting the solid angle of view. The position and axis of the BPM's detector head as well as its angle of view were specially selected based on expected average direction of particle flux with respect to the spacecraft position. The two first layers of the detecting head are made from high purity silicon PIN detectors with an area of 100 mm^2 and thickness of 100 μm and 1000 μm respectively. The last and the most deeply placed detector is based on the p-terphenyl organic scintillator optically coupled with silicon photomultiplier (SiPM). Such a multilayer detector structure in combination with dedicated coincidence logic allows data to be obtained on particle type and its energy. The detector head is connected directly to the BPM's analogue unit, containing two independent channels for silicon PIN sensors. The third separate channel dedicated for scintillator detector consists of fixed-gain amplifier, pulse shaper and digitally controlled comparator (Fig. 7). The BPM's digital unit based on FPGA (Field-Programmable Gate Array) controls the analogue unit and collects data from detectors, contains coincidence logic, forms telemetry and housekeeping frames, communicates with the

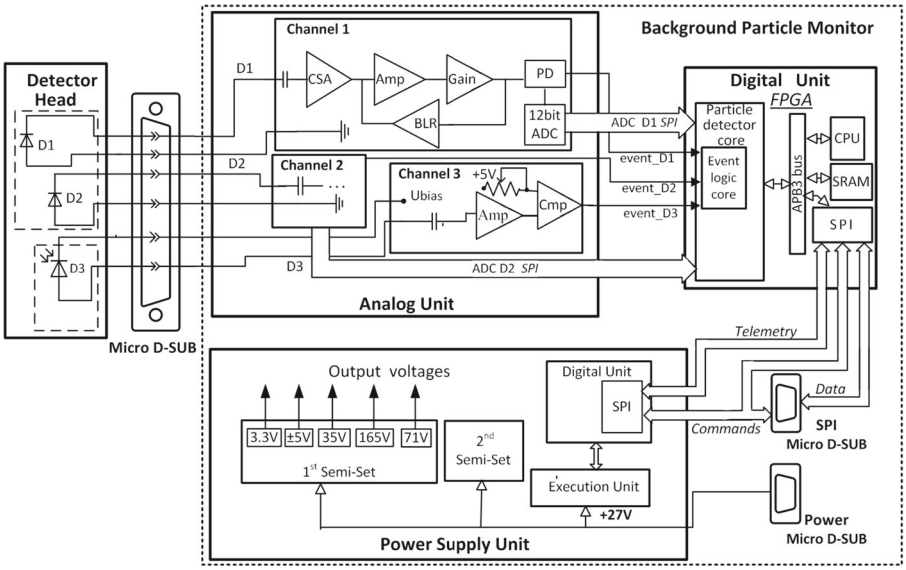

Fig. 7 Block diagram of the Background Particle Monitor electronics including power supply

ChemiX main computer and executes received telecommands. Because of the adjustable gain, the BPM can operate in one of three regimes featuring different sensitivities of individual BPM detectors. Each regime allows registration of different set of particle species from electrons up to nuclei of oxygen.

The monitor is under development at Kharkiv, Ukraine at the Institute of Radio Astronomy, NASU. The Kharkiv group has substantial experience in measurements of the energetic particle fluence and spectra present in the magnetosphere, and they have a proven record of successful detection of the radiation satellite environment on the *CORONAS-Photon* mission [STEP-F; 9]. Science objectives and more of the construction details of BPM have been summarized in [10–13].

4.2 Optical imaging system

The pin-hole imager with an aperture area of the order of 0.1 mm^2 and length 144 mm projects the real-time X-ray solar image on the CCD (as obtained through the thin graphite filter). The diameter of the solar disc at the Sun-spacecraft distance 0.3 AU will be approximately 170 pixels, while at the 1 AU the Sun will cover about 50 pixels on the CCD. The cross-section of the imager is shown in the Fig. 8 (left panel). The simulated images of the Sun with the *GOES* C1 class flare as observed at distances 0.3 and 1 AU are also presented in the Fig. 8. The images will have an intrinsic resolution of a few arcmin, enough to distinguish emission formed in the individual active regions of the corona and to observe X-ray limb brightening. The images, to be analyzed on-line by the instrument processor, will allow a region of interest (ROI) to be located within the instrument coordinate system. The ROI will normally be the brightest region of the visible X-ray corona. Flags will be passed to the motor which

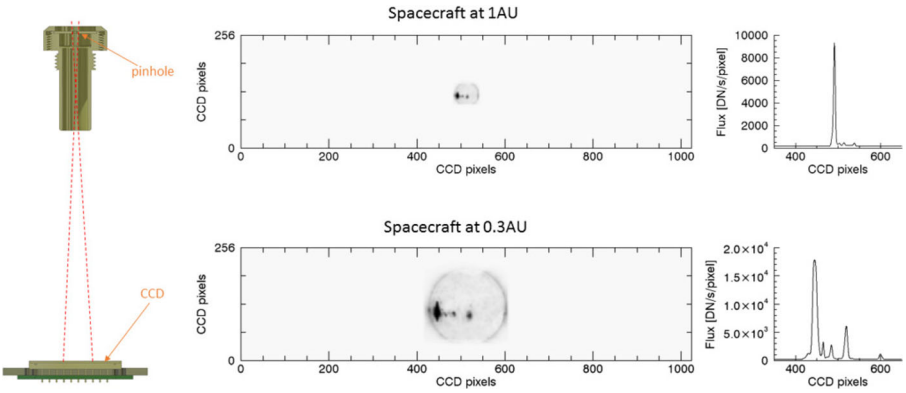

Fig. 8 *Left* The cross-section of the pin-hole imager. *Middle* The simulated images of the solar disc with the *GOES* C1 flare as seen on the CCD at the distances 0.3 and 1 AU from the Sun. *Right* The expected fluxes at horizontal cross-sections through the solar disc at the position of the brightest pixel of the corresponding image

will point the entire spectrometer towards the ROI. This action may be overridden on command from the ground if a more suitable region is selected by an observer.

4.3 Detectors and electronics

The electronic circuits used are shown in the block diagram of Fig. 9.

The detectors will consist of the eleven identical CCD detectors (manufactured by the e2v company and space-flight proven – see http://www.e2v.com/). Four detectors will sense Bragg-diffracted spectra from the spectrometer, six will sense spectra from the dopplerometer, and one will sense the image obtained by the pin-hole imager. Every CCD has a rectangular 256×1024 pixel array with pixels of size 26×26 μm. All CCDs will be passively cooled by an efficient system of heat pipes connected to an external radiator. This will allow for the CCD operating temperature to be below $\sim -20^{\circ}\,C$. The CCD system is to be developed and tested together with the Lebedev Physical Institute of the Russian Academy of Sciences (LPI RAS), Moscow.

The instrument will be equipped with a calibration system, which will allow for the calibration of the CCDs during the satellite travel along its orbit. It will consist of ten Fe^{55} radioactive sources mounted on a specially designed bars. Localization of these bars is indicated on Fig. 6. The movable platform allows the detectors to be set in a specific position, in which CCDs will be illuminated by the radioactive sources.

4.4 Filters, collimators and thermal shielding

Thermal shield and ultraviolet filters (TUVF) consisting of two identical sections are attached to the front and rear planes of spacecraft thermal shield. The main function of these two layers is to block the thermal load of solar radiation on the instrument and prevent the heat to penetrate down to the S/C. Absorption in these units effectively limit the spectral range of ChemiX to wavelengths below $\sim$ 10 Å. The

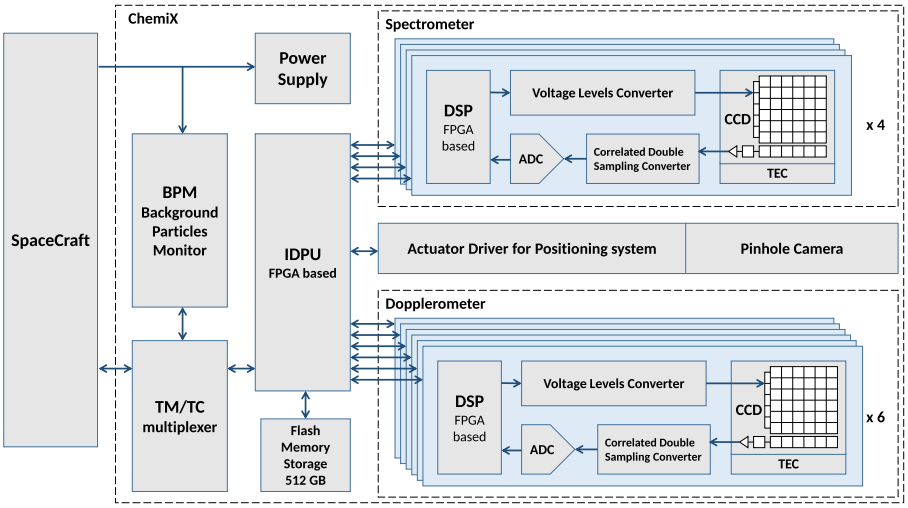

Fig. 9 Spectrometer ChemiX will be equipped with 11 CCD detectors. Each detector is connected to digital-analog front-end electronics (FEE). The FEE is controlled by small microcontroller (CoreABC) embedded into the FPGA. This approach allows to clock CCD and read photons converted to voltage. The main Instrument Data Processing Unit (IDPU) will manage storage, compressing and sending data to the satellite telemetry system (TM). The large Storage Flash Memory will store compressed data. The IDPU can be controlled from the Satellite Onboard Computer trough the telecommand system (TC). The TM/TC multiplexer connects the Background Particle Monitor (BPM) directly to TM/TC system when a block of detectors is switched off, otherwise BPM is controlled by IDPU

best candidate materials of the filters planned for use are based on thin carbon foils (graphite and/or graphene). A capillary collimator will be located immediately in front of the crystals, the main function of which will be to restrict the field of view (to < 3 arcmin^2 in both transversal directions) of solar X-rays so that individual active regions or flares can be observed.

4.5 Onboard processor, command system, data handling and telemetry

ChemiX will be controlled by an on-board computer, connected to S/C telemetry. The instrument electronics will be based on FPGA technology where possible. An important part of it will be the instrument processor-controller equipped with programs to monitor the measurements, activate the motors of the moving parts, locate the source regions on the changing-diameter solar disk, issuing flare flags, compressing the data and formatting them appropriately for the telemetry queue input. Time will be assigned to each CCD detector event (down to 1 millisecond) to allow for further analysis if requested by the ground command. A large memory buffer will be installed (up to 512 GB) to store the history of all registered events including the arrival time and the signal amplitude (for the first, second and third diffraction order events). Pre-selected parts from this data bank will be downlinked when telemetry contact allows for faster transmission rates.

5 Summary

The ChemiX instrument on the forthcoming Russian *Interhelioprobe* spacecraft is planned for launch into elliptical orbits around the Sun in 2025 and 2026. The instrument will have four channels observing Fe XXV, Ca XIX, S XV, Si XIII and Si XIV spectra as well as lines of Mg and Al and the soft X-ray continuum in the spectral range 1.5 Å – 9 Å. The diffracting crystals will be arranged in a dopplerometer configuration as for DIOGENESS [43] but unlike the DIOGENESS configuration the crystals will be bent. The use of cooled CCD detectors will give much better spectral resolution over the RESIK spectrometer on *CORONAS-F* which had position-sensitive proportional counters for the spectra detectors. A collimator placed in front of the crystals will allow the emission from individual active regions to be observed to avoid confusion from other active regions on the solar disk.

The instrument will have a Fe^{55} radioactive sources, which will allow for the calibration of the CCD "flat-field" response over the entire mission duration. The instrument will be always "on", except for initial outgassing and periods of strong SEP or CME crossings. Substantial operational autonomy will be provided at periods where limited connectivity from Earth to the spacecraft (e.g. the satellite being close to or behind the Sun) as seen from Earth.

ChemiX is under development at the Wrocław Solar Physics Division of the Polish Academy of Sciences Space Research Centre in collaboration with an international team. It is at present the only soft X-ray Bragg spectrometer planned for investigating solar activity during solar cycle 25/26, except for SolpeX polarimeter-spectrometer which is projected for mounting on the International Space Station (ISS) in 2019 [35]. The telemetry quota allocated already to ChemiX, of the order of 60 MB/day, will allow us ultimately to create the largest and most detailed database on X-ray spectra formed in high temperature, medium density plasmas typical of solar flares. This open-access database will be used not only for solar physics investigations but will also be of interest for plasma physics.

Acknowledgments We acknowledge the support from the Polish National Science Centre grants: 2011/01/M/ST9/05878, 2011/01/M/ST9/06096, and 2013/11/B/ST9/00234.

We also acknowledge use of the CHIANTI atomic database and code for Fig. 4, CHIANTI is a collaborative project involving George Mason University, University of Michigan (USA) and University of Cambridge (UK).

Appendix A: The geometry of the crystal – detector unit

The ChemiX is an X-ray spectrometer which uses bent crystals as dispersion elements. According to Bragg's law

$$2d \sin\theta = \mathrm{n}\lambda \tag{1}$$

only X-rays satisfying the Bragg condition, are reflected from the surface of the crystal. Here λ is the incident photon wavelength, d is the spacing of planes in the mono crystal wafer, θ is the incident angle with respect to the crystal plane, and n is an integer corresponding to the crystal's reflection order. Therefore, for the bent crystal,

in the 1st order reflection wavelength range $\lambda_1 - \lambda_2$ correspond to the angles $\theta_1 - \theta_2$ (see Fig. 10).

Figure 10 shows the schematic geometry of the crystal-detector unit of the ChemiX spectrometer. The plot is in the rectangular coordinate system with origin at the centre of the crystal curvature. The solar radiation, coming from above, is diffracted by the bent crystal with a radius of curvature r and the surface marked with a thick black solid line. After Bragg reflection it falls on a position-sensitive CCD detector, indicated in the figure with the thick yellow line. ChemiX contains a collimator, which narrows the field of view of the instrument. Therefore, we consider the possibility of observing the radiation deflected at an angle of ± 3 arcmin from the rays coming from the center of symmetry. This is so called "offset angle", labeled as φ. Two extreme rays that can fall on the crystal are marked as blue and red lines in the Fig. 10. They fall on the crystal at points with coordinates:

$$x_1 = r \cos(\theta_1 - \varphi) \tag{2}$$

$$y_1 = r \sin(\theta_1 - \varphi) \tag{3}$$

and

$$x_2 = r \cos(\theta_2 + \varphi) \tag{4}$$

$$y_2 = r \sin(\theta_2 + \varphi) \tag{5}$$

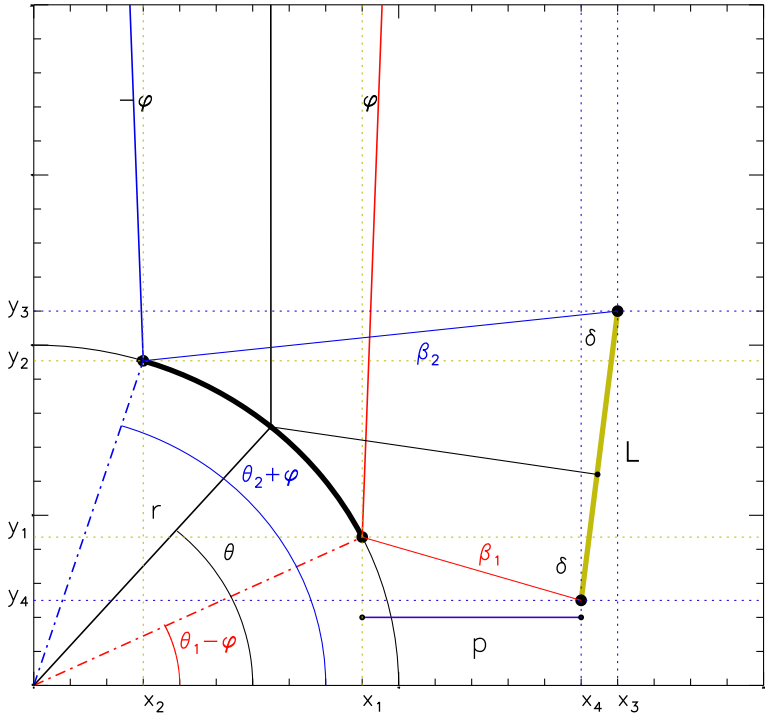

Fig. 10 Schematic geometry of the crystal-detector section with definition of the angles and other important parameters used

For a given type of crystal (i.e. specific crystal lattice spacing d), the offset angle φ, the detector length L and the desired wavelength range, our software determines the optimal geometry of the crystal–detector system. It calculates the crystal curvature, r , the positions of the edges of the crystal (x_1, y_1) and (x_2, y_2) and the positions of the edges of the detector (x_3, y_3) and (x_4, y_4).

Because we have nine unknowns we would need nine equations to uniquely solve the system. In addition to the (2–5) for a geometry shown in Fig. 10 we can write the following set of equation for the positions of the detector edges:

$$y_3 = a_2 x_3 + b_2 \tag{6}$$

$$y_3 = a_L x_3 + b_L \tag{7}$$

$$y_4 = a_1 x_4 + b_1 \tag{8}$$

$$y_4 = a_L x_4 + b_L \tag{9}$$

Here a_1, b_1, a_2 and b_2 are the coefficients (a- the slope, b- the y-intercept of the line in the form $y = ax + b$) of lines connecting the points of incidence of the extreme rays at the ends of the detector with the corresponding edges of the crystal. They can be established from the geometrical relationships between the angles in the system:

$$a_1 = \tan(\beta_1) = \tan(2\theta_1 - 90^\circ - \varphi) \tag{10}$$

$$a_2 = \tan(\beta_2) = \tan(2\theta_2 - 90^\circ + \varphi) \tag{11}$$

$$b_1 = y_1 - x_1 \tan(\beta_1) = r\sin(\theta_1 - \varphi) - r\cos(\theta_1 - \varphi)\tan(2\theta_1 - 90^\circ - \varphi) \tag{12}$$

$$b_2 = y_2 - x_2 \tan(\beta_2) = r\sin(\theta_2 + \varphi) - r\cos(\theta_2 + \varphi)\tan(2\theta_2 - 90^\circ + \varphi) \tag{13}$$

We have now eight equations, but we introduced two additional variables, a_L and b_L. Those coefficients define the straight line on which the detector lies. Thus three more equations are needed.

Firstly we can use the known length of the detector to write:

$$L^2 = (x_4 - x_3)^2 + (y_4 - y_3)^2 \tag{14}$$

For an optimal arrangement of the crystal – detector unit the angles δ between the extreme rays and the detector are the same (see: Fig. 10). Therefore we can write:

$$\frac{a_1 - a_L}{1 + a_1 a_L} = \frac{a_L - a_2}{1 + a_2 a_L} \tag{15}$$

Left and right sides of this equation are the expression on tangent of angle between detector and the extreme rays.

Due to the CCD's housing we need some free space between the crystal and detector and so, we need to introduce p parameter- the distance between the closest part of the crystal and the detector. The last needed equation can be therefore written using this known parameter. Depending on the slope of the detector the equation may take one of the two forms:

$$x_4 = x_1 + p \tag{16}$$

when the detector is positioned as shown in Fig. 10 (a_L>0), or

$$x_3 = x_1 + p \tag{17}$$

When x_3 is closer to the crystal than x_4 (a_L<0).

Ultimately we have eleven unknown values and eleven equations (2–9, 14, 15 and one of 16 or 17) so the problem can be solve unambiguously. Minimalization of parameter p or equalization of angles δ, described by (15–17) can be treated as criteria for the optimization of the crystal–detector design but they are necessary for the closure of system of equations to be solved.

Firstly we determinate the radius of curvature. Starting with (14) we substitute the y_3 and y_4 into the (7) and (9). After transform we can write:

$$x_4^2(1+a_L^2)+x_4[-2x_3(1+a_L^2)]+[x_3(1+a_L^2)-L^2]=0 \tag{18}$$

which allow us to determinate the x_4:

$$x_4 = x_3 + S \tag{19}$$

Here:

$$S=\pm\frac{\sqrt{(1+a_L^2)L^2}}{(1+a_L^2)} \tag{20}$$

On the other hand using the (6), (7), (8) and (9) we have:

$$a_1x_4+b_1-a_Lx_4=a_2x_3+b_2-a_Lx_3 \tag{21}$$

We can solve it for x_3 and insert the (19) to get:

$$x_3=\frac{b_2-b_1}{a_1-a_2}+S\frac{a_L-a_1}{a_1-a_2} \tag{22}$$

Now we can use appropriate (16) or (17) following by (12), (13) and (6) to obtain the relevant equations for crystal radius of curvature:

$$r=\frac{p(a_1-a_2)-S(a_1-a_2)-S(a_L-a_1)}{\sin(\theta_2+\varphi)-\sin(\theta_1-\varphi)-\mathrm{a}_2\cos(\theta_2+\varphi)+\mathrm{a}_2\cos(\theta_1-\varphi)} \tag{23}$$

$$r=\frac{p(a_1-a_2)-S(a_L-a_1)}{\sin(\theta_2+\varphi)-\sin(\theta_1-\varphi)-\mathrm{a}_2\cos(\theta_2+\varphi)+\mathrm{a}_2\cos(\theta_1-\varphi)} \tag{24}$$

In the next step we solve the (15) with respect to variable a_L. It is a quadratic equation which gives us two solutions. But from (16) and (17) we know, that the (23) works for $a_L > 0$ while the (24) works for $a_L < 0$. This allow us to choose appropriate solution of (15) and use it in selected equation for r. In this way we get four values for crystal radius of curvature. From the possible solutions of (23) and (24) we choose those, for which the value of radius of curvature are positive (convex crystal) and calculate the corresponding crystal and detector positions (x_3, y_3) and (x_4, y_4). Finally we chose an arrangement that give as small as possible size of crystal–detector unit.

Now we need to solve an inverse task, i.e. to calculate wavelengths corresponding to each pixel (x, y) of the detector. Without loss of generality we can assume that X-rays of given wavelength fall on the crystal at the coordinates (x_1, y_1). Points (x_1, y_1) and (x, y) define straight line with a slope a:

$$y-y_1=a(x-x_1) \tag{25}$$

Using (10) for a:

$$a = \tan(2\theta - \varphi - 90^\circ) = -\frac{\cos(2\theta - \varphi)}{\sin(2\theta - \varphi)} \tag{26}$$

and (2) and (3) for x_1 and y_1, we can obtain:

$$y - r\sin(\theta - \varphi) = -\frac{\cos(2\theta - \varphi)}{\sin(2\theta - \varphi)}[\mathrm{x} - \mathrm{r}\cos(\theta - \varphi)] \tag{27}$$

This equation can be transformed into:

$$\begin{gathered} 2\sin\theta\cos\theta(\mathrm{y}\cos\varphi + \mathrm{x}\sin\varphi) + 2\cos^2\theta(\mathrm{x}\cos\varphi - \mathrm{y}\sin\varphi) - (\mathrm{x}\cos\varphi - \mathrm{y}\sin\varphi) \\ = 2r\cos^3\theta\cos^2\varphi - \mathrm{r}\cos\theta\cos^2\varphi + 2\sin\theta\cos^2\theta\sin\varphi\cos\varphi + 2\mathrm{r}\sin\theta\cos^2\theta\sin\varphi\cos\varphi \\ -r\sin\theta\sin\varphi\cos\varphi + 2\mathrm{r}\sin^2\theta\cos\theta\sin^2\varphi \\ +2r\sin^2\theta\cos\theta\cos^2\varphi - 2\mathrm{r}\sin\theta\cos^2\theta\sin\varphi\cos\varphi \\ +r\sin\theta\cos\varphi\sin\varphi - 2\mathrm{r}\sin\theta\cos^2\theta\sin\varphi\cos\varphi + 2\mathrm{r}\cos^3\theta\sin^2\varphi - \mathrm{r}\cos\theta\sin^2\varphi \end{gathered} \tag{28}$$

We introduce the designations:

$$A = y\cos\varphi + \mathrm{x}\sin\varphi \tag{29}$$

and

$$B = x\cos\varphi - \mathrm{y}\sin\varphi \tag{30}$$

After making the substitution and simplification we obtain the fourth degree equation:

$$\cos^4\theta\,[4(A^2 + B^2)] + \cos^3\theta\,[-4rB] + \cos^2\theta\,[-4(\mathrm{A}^2 + \mathrm{B}^2) + \mathrm{r}^2] + \cos\theta\,[2\mathrm{rB}] + [\mathrm{B}^2] = 0 \tag{31}$$

which may be solved using the FZ_ROOTS function available in IDL. This allows us to calculate for a chosen crystal-detector arrangement the X-ray wavelength range that corresponds to every detector bin physical positions limits.

Appendix B: The flux determination

The Bragg law describes the X-rays diffraction on the crystal. Unfortunately this law does not describe the complicated Bragg diffraction-interference perfectly. In the "real" case, the monochromatic X-ray beam become scattered after "reflection" from the crystal. The crystal rocking curve (see Fig. 11) shows the dependence between the reflection angle and the reflectivity, R:

$$R = \frac{I_0}{I}$$

where I and I_0 are the incident and diffracted fluxes respectively. The $\theta - \theta_0$ is the difference between the real reflected angle and the angle resulting from the Bragg law. The rocking curve for perfect crystals in the Bragg case has been discussed by many authors. A list of references may be found in books [e.g. 20, 49] or in the articles [4,

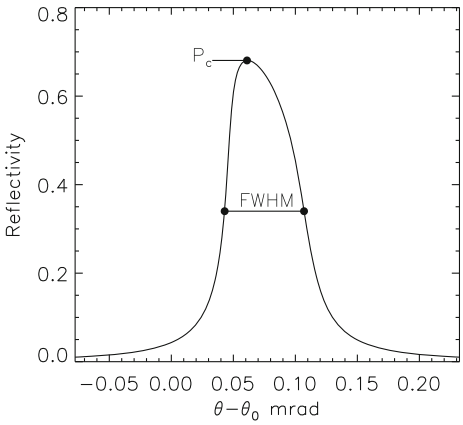

Fig. 11 The rocking curve of the Si 111 bent crystal at energy 3800 eV (λ=3.26Å). It was obtained using XOP software [32]

17] or [6]. The characteristic features of the rocking curve are the full width at half maximum (FWHM), the peak reflectivity (P_c) and the integral reflectivity (R_c):

$$\begin{aligned} R_c(\theta) &= \int R(\theta)\, d\theta = \int R(\theta(\lambda))\, \frac{d\theta}{d\lambda} d\lambda \\ &= \int R(\lambda)\, \frac{d\theta}{d\lambda} d\lambda = \int R(\lambda) \frac{1}{2d\cos\theta}\, d\lambda \approx \frac{1}{2d\cos\theta} \int R(\lambda)\, d\lambda \\ &= \frac{1}{2d\cos\theta} R_c(\lambda) = \frac{\sin\theta}{2d\cos\theta\sin\theta} R_c(\lambda) = \frac{\mathrm{tg}\,\theta}{\lambda} R_c(\lambda) \end{aligned} \tag{32}$$

Thus

$$R_c(\lambda) = R_c(\theta)\lambda \mathrm{ctg}\theta \tag{33}$$

To interpret the observing spectra we need to know the instrument response function, which will relate the rates [cts/s/bin] observed in each spectral bin into absolute fluxes units [photons/cm^2/s/Å]. Let us consider an infinitesimally small fragment of crystal of length dl in the dispersion plane and width W. This elements supplies the detector with the flux:

$$dN = FE\, dA \tag{34}$$

here E is the efficiency function, that contain the instrument filters' transmission function, the collimator transmission function and the detector efficiency. F is given by:

$$F = \int_0^\infty f(\lambda) R(\lambda) d\lambda \tag{35}$$

where $f(\lambda)$ is the flux on-axis point source and $R(\lambda)$ is the crystal reflectivity. dA is the area of the considered segment of crystal. For a point source on the line-of-sight we can write:

$$dA = A_0 \sin\theta = \mathrm{W\,dl} \sin\theta \tag{36}$$

Because

$$dl = r d\theta \tag{37}$$

and

$$\frac{dl}{d\lambda} = \frac{r\,d\theta}{d\lambda} = \frac{r}{2d\cos\theta} \tag{38}$$

the area can be written as:

$$dA = \frac{W\,r\sin\theta}{2d\cos\theta}d\lambda \tag{39}$$

We can therefore rewrite (34) as:

$$dN = E\frac{W\,r\sin\theta}{2d\cos\theta}d\lambda\int_0^\infty f(\lambda)R(\lambda)d\lambda \tag{40}$$

Equation (40) was used to calculate expected fluxes on the synthetic spectrum (see Fig. 4).

References

1. Acton, L.W., Finch, M.L., Gilbreth, C.W., Culhane, J.L., Bentley, R.D., Bowles, J.A., Guttridge, P., Gabriel, A.H., Firth, J.G., Hayes, R.W.: The soft X-ray polychromator for the solar maximum mission. Solar Phys. **65**, 53–71 (1980). doi:10.1007/BF00151384
2. Antia, H.M., Basu, S.: Determining solar abundances using helioseismology. Astrophys. J. **644**, 1292–1298 (2006). doi:10.1086/503707
3. Antonucci, E., Gabriel, A.H., Dennis, B.R.: The energetics of chromospheric evaporation in solar flares. Astrophys. J. **287**, 917–925 (1984). doi:10.1086/162749
4. Batterman, B.W., Cole, H.: Dynamical diffraction of X-rays by perfect crystals. Rev. Mod. Phys. **36**, 681 (1964). doi:10.1103/RevModPhys.36.681
5. Bradshaw, S.J., Raymond, J.: Collisional and radiative processes in optically thin plasmas. Space Sci. Rev. **178**, 271–306 (2013). doi:10.1007/s11214-013-9970-0
6. Bucksch, R., Otto, J., Renninger, M.: Die 'Diffraction Pattern' des Idealkristalls fü. Acta Crystallogr. **23**, 507–511 (1967). doi:10.1107/S0365110X6700310X
7. Culhane, J.L., Hiei, E., Doschek, G.A., Cruise, A.M., Ogawara, Y., Uchida, Y., Bentley, R.D., Brown, C.M., Lang, J., Watanabe, T., Bowles, J.A., Deslattes, R.D., Feldman, U., Fludra, A., Guttridge, P., Henins, A., Lapington, J., Magraw, J., Mariska, J.T., Payne, J., Phillips, K.J.H., Sheather, P., Slater, K., Tanaka, K., Towndrow, E., Trow, M.W., Yamaguchi, A.: The bragg crystal spectrometer for SOLAR-A. Solar Phys. **136**, 89–104 (1991). doi:10.1007/BF00151696
8. Doschek, G.A., Kreplin, R.W.: Feldman, U.: High-resolution solar flare X-ray spectra. Astrophys. J. Lett. **233**, L157–L160 (1979). doi:10.1086/183096
9. Dudnik, O.V.: Investigation of the Earths radiation belts in May 2009 at the low orbit satellite with the STEP-F instrument. Space Sci. Technol. **16**, 12–28 (2010). doi:10.1086/183096. In Russian
10. Dudnik, O.V., Kurbatov, E., Avilov, A., Prieto, M., Sanchez, S., Spassky, A., Titov, K., Sylwester, J., Gburek, S., Podgórski, P.: Results of the first tests of the SIDRA satellite-borne instrument breadboard model. Problems of Atomic Science and Technology, 3 (2013)
11. Dudnik, O.V., Kurbatov, E., Sylwester, J., Siarkowski, M., Kowaliński, M., Titov, K., Andryushenko, L., Zajtsevsky, I., Valtonen, E.: Development of small-sized SIDRA device for monitoring of charged particle fluxes in space, pp. 62–67. Publ. House "Akademperiodika" (2014). In Russian
12. Dudnik, O.V., Kurbatov, E., Tarasov, V., Andryushenko, L., Zajtsevsky, I., Sylwester, J., Bąkała, J., Kowaliński, M.: Background particle detector for the solar X-ray photometer ChemiX of space mission "Interhelioprobe": an adjustment of breadboard model modules. Kosmichna Nauka I Tekhnologiya **21**, 3–14 (2015). ISSN 1561-8889, In Russian
13. Dudnik, O.V., Prieto, M., Kurbatov, E., Sanchez, S., Titov, K., Sylwester, J., Gburek, S., Podgórski, P.: Functional capabilities of the breadboard model of SIDRA satellite-borne instrument. Problems of Atomic Science and Technology **3** (2013)

14. Dzifčáková, E., Kulinová, A., Chifor, C., Mason, H.E., Del Zanna, G., Sylwester, J., Sylwester, B.: Nonthermal and thermal diagnostics of a solar flare observed with RESIK and RHESSI. Astron. Astrophys. **488**, 311–321 (2008). doi:10.1051/0004-6361:20078367
15. Feldman, U., Doschek, G.A., Kreplin, R.W., Mariska, J.T.: High-resolution X-ray spectra of solar flares. IV - General spectral properties of M type flares. Astrophys. J. **241**, 1175–1185 (1980). doi:10.1086/158434
16. Fludra, A., Bentley, R.D., Lemen, J.R., Jakimiec, J., Sylwester, J.: Turbulent and directed plasma motions in solar flares. Astrophys. J. **344**, 991–1003 (1989). doi:10.1086/167866
17. Hirsch, P.B., Ramachandran, G.N.: Intensity of X-ray reflexion from perfect and mosaic absorbing crystals. Acta Crystallographica **3**, 187–194 (1950). doi:10.1107/S0365110X50000458
18. Jakimiec, J., Fludra, A., Lemen, J.R., Dennis, B.R., Sylwester, J.: Investigations of turbulent motions and particle acceleration in solar flares. Adv. Space Res. **6**, 191–194 (1986). doi:10.1016/0273-1177(86)90143-2
19. Jakimiec, J., Korneev, V.V., Krutov, V.V., Zhitnik, I.A., Płocieniak, S., Sylwester, B., Sylwester, J.: Analysis of the intensities and profiles of the spectral line Mg XII 8.42 Å in the solar X-ray spectrum. Solar Phys. **44**, 391–401 (1975). doi:10.1007/BF00153218
20. James, W.R.: The optical principles of the diffraction of X-rays. G. Bell and Sons, Inc., London (1950)
21. Krutov, V.V., Korneev, V.V., Karev, U.I., Lomkova, V.M., Oparin, S.N., Urnov, A.M., Zhitnik, I.A., Bromboszcz, G., Siarkowski, M., Sylwester, J.: Analysis of the high-resolution X-ray spectra obtained aboard the Intercosmos 16 satellite. I - Identification of the lines in the 9.14-9.33 A spectral region. Solar Phys. **73**, 105–119 (1981). doi:10.1007/BF00153148
22. Kulinová, A., Dzifčáková, E., Sylwester, B., Sylwester, J.: Non-thermal Diagnostics of a Flare Observed by RESIK. Central European Astrophysical Bulletin **33**, 243–252 (2009)
23. Kuznetsov, V., Zelenyi, L.: The interhelioprobe mission for solar and heliospheric studies. In: 40th COSPAR Scientific Assembly, *COSPAR Meeting*. To be published, vol. 40, p. 1721 (2014)
24. Kuznetsov, V.D., Zelenyi, L.M.: Space projections on solar-terrestrial physics. Geomagn. Aeron. **49**, 1137–1147 (2009). doi:10.1134/S0016793209080209
25. Laming, J.M.: Non-Wkb models of the first ionization potential effect: implications for solar coronal heating and the coronal helium and neon abundances. Astrophys. J. **695**, 954–969 (2009). doi:10.1088/0004-637X/695/2/954
26. Laming, J.M.: The FIP and inverse FIP effects in solar and stellar coronae. Living Reviews in Solar Physics **12**, 2 (2015). doi:10.1007/lrsp-2015-2
27. Marsch, E., Harrison, R., Pace, O., Antonucci, E., Bochsler, P., Bougeret, J.L., Fleck, B., Langevin, Y., Marsden, R., Schwenn, R., Vial, J.C.: Solar Orbiter, a high-resolution mission to the Sun and inner heliosphere. In: Battrick, B., Sawaya-Lacoste, H., Marsch, E., Martinez Pillet, V., Fleck, B., Marsden, R. (eds.) Solar Encounter. Proceedings of the First Solar orbiter Workshop, vol. 493, p. D11. ESA Special Publication (2001)
28. Oraevsky, V.N., Galeev, A.A., Kuznetsov, V.D., Zelenyi, L.M.: Solar orbiter and russian aviation and space agency interhelioprobe. In: Battrick, B., Sawaya-Lacoste, H., Marsch, E., Martinez Pillet, V., Fleck, B., Marsden, R. (eds.) Solar Encounter. Proceedings of the First Solar Orbiter Workshop, vol. 493, pp. 95–108. ESA Special Publication (2001)
29. Phillips, K.J.H., Pike, C.D., Lang, J., Watanbe, T., Takahashi, M.: Iron K beta line emission in solar flares observed by YOHKOH and the solar abundance of iron. Astrophys. J. **435**, 888–897 (1994). doi:10.1086/174870
30. Phillips, K.J.H., Sylwester, J., Sylwester, B., Kuznetsov, V.D.: The solar X-ray continuum measured by RESIK. Astrophys. J. **711**, 179–184 (2010). doi:10.1088/0004-637X/711/1/179
31. Płocieniak, S., Sylwester, J., Kordylewski, Z., Sylwester, B.: Determination of wavelengths and line shifts based on X-ray spectra from Diogeness. In: Wilson, A. (ed.) Solar Variability: from Core to Outer Frontiers, vol. 506, pp. 963–966. ESA Special Publication (2002)
32. Sachez del Rio, M., Dejus, R.: XOP v2.4: recent developments of the X-ray optics software toolkit. In: Proceedings of SPIE 8141, advances in computational methods for X-ray optics II, vol. 8141 (2011). doi:10.1117/12.893911
33. Serenelli, A.M., Basu, S., Ferguson, J.W., Asplund, M.: New solar composition: the problem with solar models revisited. Astrophys. J. Lett. **705**, L123–L127 (2009). doi:10.1088/0004-637X/705/2/L123
34. Siarkowski, M., Sylwester, J., Bromboszcz, G., Korneev, V.V., Mandelshtam, S.L., Oparin, S.N., Urnov, A.M., Zhitnik, I.A., Vasha, S.: Analysis of the high resolution Mg XI X-ray spectra. II -

Physical parameters of the plasma in active region McMath 14352. Solar Phys. **77**, 183–203 (1982). doi:10.1007/BF00156104
35. Stęślicki, M., Sylwester, J., Siarkowski, M., Kowaliński, M., Płocieniak, S., Bąkała, J., Szaforz, Ż., Kuzin, S.: Soft X-ray solar polarimeter-spectrometer. In: 19th Polish-Slovak-Czech Optical Conference on Wave and Quantum Aspects of Contemporary Optics, vol. 9441. SPIE Proceedings (2014). doi:10.1117/12.2176043
36. Sylwester, B., Faucher, P., Jakimiec, J., Krutov, V.V., McWhirter, R.W.P.: Investigation of the Mg XII 8.42 A doublet in solar flare spectra. Solar Phys. **103**, 67–87 (1986). doi:10.1007/BF00154859
37. Sylwester, B., Phillips, K.J.H., Sylwester, J., Kepa, A.: Silicon abundance from RESIK solar flare observations. Solar Phys. **283**, 453–461 (2013). doi:10.1007/s11207-013-0250-7
38. Sylwester, B., Sylwester, J., Phillips, K.J.H.: X-ray studies of flaring plasma. J. Astrophys. Astron. **29**, 147–150 (2008). doi:10.1007/s12036-008-0017-y
39. Sylwester, B., Sylwester, J., Phillips, K.J.H.: Soft X-ray coronal spectra at low activity levels observed by RESIK. Astron. Astrophys. **514**, A82 (2010). doi:10.1051/0004-6361/200912907
40. Sylwester, B., Sylwester, J., Phillips, K.J.H., Kepa, A., Mrozek, T.: Solar flare composition and thermodynamics from RESIK X-ray spectra. Astrophys. J. **787**, 122 (2014). doi:10.1088/0004-637X/787/2/122
41. Sylwester, J., Farnik, F.: Diogeness - Soft X-ray spectrometer-photometer for studies of flare energy balance. Bulletin of the Astronomical Institutes of Czechoslovakia **41**, 149–157 (1990)
42. Sylwester, J., Gaicki, I., Kordylewski, Z., Kowaliński, M., Nowak, S., Płocieniak, S., Siarkowski, M., Sylwester, B., Trzebiński, W., Bakała, J., Culhane, J.L., Whyndham, M., Bentley, R.D., Guttridge, P.R., Phillips, K.J.H., Lang, J., Brown, C.M., Doschek, G.A., Kuznetsov, V.D., Oraevsky, V.N., Stepanov, A.I., Lisin, D.V.: RESIK: a bent crystal X-ray spectrometer for studies of solar coronal plasma composition. Solar Phys. **226**, 45–72 (2005). doi:10.1007/s11207-005-6392-5
43. Sylwester, J., Kordylewski, Z., Płocieniak, S., Siarkowski, M., Kowaliński, M., Nowak, S., Trzebiński, W., Stęślicki, M., Sylwester, B., Stańczyk, E., Zawerbny, R., Szaforz, Ż., Phillips, K.J.H., Fárník, F., Stepanov, A.: X-ray flare spectra from the DIOGENESS spectrometer and its concept applied to ChemiX on the interhelioprobe spacecraft. Solar Phys. (2015). doi:10.1007/s11207-014-0644-1
44. Sylwester, J., Sylwester, B., Landi, E., Phillips, K.J.H., Kuznetsov, V.D.: Determination of K, Ar, Cl, S, Si and Al flare abundances from RESIK soft X-ray spectra. Adv. Space Res. **42**, 838–843 (2008). doi:10.1016/j.asr.2007.05.060
45. Sylwester, J., Sylwester, B., Phillips, K.J.H., Kuznetsov, V.D.: Highly ionized potassium lines in solar X-ray spectra and the abundance of potassium. Astrophys. J. **710**, 804–809 (2010). doi:10.1088/0004-637X/710/1/804
46. Sylwester, J., Sylwester, B., Phillips, K.J.H., Kuznetsov, V.D.: The solar flare sulfur abundance from RESIK observations. Astrophys. J. **751**, 103 (2012). doi:10.1088/0004-637X/751/2/103
47. Tanaka, K., Watanabe, T., Nishi, K., Akita, K.: High-resolution solar flare X-ray spectra obtained with rotating spectrometers on the HINOTORI satellite. Astrophys. J. Lett. **254**, L59–L63 (1982). doi:10.1086/183756
48. Testa, P.: Element abundances in X-ray emitting plasmas in stars. Space Sci. Rev. **157**, 37–55 (2010). doi:10.1007/s11214-010-9714-3
49. Zachariasen, W.H.: Theory of X-ray diffraction in crystals. John Wiley and Sons, Inc., New York (1945)
50. Zarro, D.M., Lemen, J.R.: Conduction-driven chromospheric evaporation in a solar flare. Astrophys. J. **329**, 456–463 (1988). doi:10.1086/166391